Pergamon

Geochimica et Cosmochimica Acta, Vol. 61, No. 4, pp. 707–718, 1997

0016-7037/97 $17.00 + .00

PII S0016-7037(96)00376-6

An AEM-TEM study of nanometer-scale mineral associations in an aquifer sand: Implications for colloid mobilization

CHRISTOPHER H. SWARTZ,[1] APRIL L. ULERY,[2] and PHILIP M. GSCHWEND[1]

[1]Ralph M. Parsons Laboratory, Department of Civil and Environmental Engineering, Massachusetts Institute of Technology, Cambridge, Massachusetts 02139, USA
[2]U.S. Salinity Laboratory, Riverside, California 92507, USA

(*Received May* 2, 1996; *accepted in revised form November* 3, 1996)

Abstract—Analytical and transmission electron microscopy (AEM-TEM) techniques were used to identify mineral juxtapositions at the nanometer-scale in the interstitial matrix of a shallow, Southeastern Coastal plain aquifer sand (Georgetown, South Carolina, USA). In doing so, we sought to infer particle-particle interaction mechanisms holding the matrix intact. The aquifer is a fine-to-medium quartz sand with approximately 12% by weight <63 μm size fraction composing the interstitial matrix. The clay-size fraction contains kaolinite, goethite, gibbsite, and vermiculite. The arrangement of the clay minerals is that of a framework of face-associated domains. Selective extraction revealed that goethite constituted 95% by weight of the free iron oxyhydroxides in the <63 μm size fraction, but AEM-TEM and high resolution TEM (HRTEM) indicated that the goethite occurred only in discrete aggregates among the clays. Conversely, the remaining 5% of the free iron oxyhydroxides comprised an amorphous iron phase which was found to be distributed throughout the matrix and directly associated with the clay particles. This evidence suggests that the amorphous iron oxyhydroxide phase could act as an effective binding intermediary among the clay-clay associations, possibly electrostatically or through bond linkages with the clay surfaces. In addition, HRTEM indicated the presence of another amorphous phase which appeared to hold the clay particle aggregates in a cementitious web. AEM suggested that this amorphous phase was silicon enriched, probably biogenic opal. This evidence suggests that instigating dissolution of the opaline silica phase may be necessary to induce substantial colloid mobilization in this aquifer sediment.

1. INTRODUCTION

The existence of mobile colloidal phases in groundwaters has become increasingly recognized (Gschwend and Reynolds, 1987; Short et al., 1988; Degueldre et al., 1989; Backhus et al., 1993). It has been suggested that, in some instances, colloidal material may play an important role in the facilitated subsurface transport of contaminants (McCarthy and Zachara, 1989; McDowell-Boyer, 1992). For example, colloids have been implicated in the transport of radionuclides (Buddemeier and Hunt, 1988; Penrose et al., 1990) and heavy metals (Newman et al., 1993; Kaplan et al., 1995).

Concomitantly, greater attention has been given to the fine-grained inorganic material which often coats and fills interstitial voids between primary grains (e.g., quartz) in aquifer sediments. It has become evident that these matrices of clay-size mineral particles can serve as release reservoirs for colloidal phases to groundwaters (Ryan and Gschwend, 1990; Kaplan et al., 1993). The origin of this material is commonly ascribed to transport and deposition of clay-size material or to authigenic formation (Hendershot and Lavkulich, 1983; Sposito, 1984). The weathering products and transported material are often reprecipitated as amorphous or crystalline iron, manganese, and aluminum sesquioxide coatings (Schwertmann and Taylor, 1989; Wang et al., 1993) and phyllosilicate minerals such as kaolinite are commonly intimately associated with these sesquioxides (Ryan and Gschwend, 1992; Malengreau et al., 1994). Elucidation of the mechanisms which induce release of these inorganic colloids from immobile sediment matrices to moving groundwater appears necessary to predict accurately subsurface contaminant transport.

Based on recent investigations, mineral particles in coatings and matrix appear to be mobilized upon subjecting a sediment to chemical perturbations in pore fluid chemistry (Cerda, 1987; McDowell-Boyer, 1992; Ryan and Gschwend, 1994; Seaman et al., 1995). These perturbations include changes in pH, E_H, ionic strength, and cation chemistry. It has been hypothesized that, in many instances, coatings and matrix material are bound in sediment by electrostatic forces existing between mineral surfaces of fixed (e.g., kaolinite faces) and variable charge (e.g., kaolinite edges, free oxyhydroxides of Fe and Al) (Ryan and Gschwend, 1994; Seaman et al., 1995). However, the necessity of dissolution of cementitious phases has been implicated in colloid release also (Gschwend et al., 1990; Ryan and Gschwend, 1990; Ronen et al., 1992).

Transmission electron microscopy (TEM) and analytical electron microscopy (AEM) techniques have been used to investigate the actual physical/spatial associations between clay-size phases in sediment matrices. Bennett et al. (1981) used TEM to determine whether clay fabrics correlated with physico-chemical forces thought to drive the arrangement of particles in marine sediment microstructures. Likewise, TEM has been used to study the nature and orientation of clay particles and location of organic matter in an aggregated, tropical, weathered soil (Santos et al., 1989).

We utilized AEM-TEM and high resolution TEM (HRTEM) to investigate the chemical composition and inti-

mate associations among inorganic phases in samples of a representative aquifer sediment and in colloid samples mobilized from the sediment matrix to gain insight into its inorganic colloid release behavior. In particular, we focused on characterizing the distribution and crystalline nature of the free oxyhydroxides of Fe in the interstitial matrix because these Fe phases have been hypothesized to be major binding agents of aquifer fines (Ryan and Gschwend, 1990; Ryan and Gschwend, 1992). In addition, we sought to determine if other free oxyhydroxide components, such as amorphous siliceous material, are present. Our objective was to use the data obtained to determine which phase(s) might play an effective role in holding the interstitial fines together.

2. EXPERIMENTAL

2.1. Sediment Characterization

Sediments used in this investigation were collected from a site on the grounds of the Baruch Forest Sciences Institute, Georgetown, South Carolina, USA. This site has been used in the past to study dissolved organic carbon (DOC) mobility and iron redox chemistry in the shallow, unconfined aquifer that is present there (Liang et al., 1993; McCarthy et al., 1993). This aquifer is part of the Southeastern Coastal Plain aquifer system and is approximately 3 m thick. The aquifer is composed of an iron oxide-coated, fine beach sand deposit of marine origin, approximately 100,000 years old, and is underlain by a 1 m thick clay layer (Williams and McCarthy, 1991). The water table is typically 1 m below the surface at the site.

Sediment was obtained from the C horizon at a depth of 2.0–2.4 m during collection of a continuous core by hollow stem auger at the site in June, 1993. Drilling fluids were not used during the coring procedure. The sample was placed in a sealed, plastic bag and refrigerated for later analysis. The coring took place in an oxidized zone of the aquifer, several hundred meters hydraulically upgradient of the study site of Liang et al. (1993).

2.1.1. Size Fractionation

Samples of the sediment were size fractionated for use in characterizing the mineralogy, total Fe, free oxyhydroxides of Fe and Al, and opaline silica present in each fraction. The <1000 μm fraction was separated into five fractions by wet sieving: 1000–500, 500–250, 250–125, 125–63, and <63 μm. Sieving was carried out using polyethylene sieves and artificial groundwater chemically mimicking that found at the site (30 μM Mg; 150 μM Na; 10 μM K; 30 μM Ca; 30 μM SO_4; 190 μM Cl; 30 μM HCO_3; pH = 5.2). All solutions used in investigating the physical and chemical properties of the sediment were prepared with Milli-Q purified water (Millipore) and reagent grade chemicals. A <2 μm fraction was obtained by the pipet method from sedimentation of a sample of the <63 μm fraction (Gee and Bauder, 1986).

2.1.2. Heavy mineral separation

Heavy minerals were separated from the size fractions by density using bromoform. Five to ten grams of each of the fractions were placed in a separatory funnel with 50 mL of bromoform. Material with density greater than 2.89 g/cm^3 was allowed to settle, collected on filter paper, washed with acetone to remove the bromoform, and allowed to air dry.

2.1.3. Mineral characterization

X-ray diffraction (XRD) was used to identify mineral phases in the <2 μm and heavy mineral fractions. Suspensions of the <2 μm fraction were centrifuged at 3400 g for 15 min to create a paste which was applied to glass slides. The heavy mineral fractions were crushed to a powder and applied to glass slides with double sided tape. Samples were CuKα irradiated using a Rigaku RU300 diffractometer operating under the following conditions: 50 kV, 200 mA, 0.5° divergence slit, 0.3 mm receiving slit. The diffraction patterns were obtained in the range 5–80° 2θ at a scan speed of 5°/min. Vermiculite was identified after collapse of the 1.4 nm d-spacing upon K-saturation at room temperature.

Kaolinite and gibbsite were quantified by thermal gravimetric analysis using a DuPont 9900 Thermal Analyzer (Wilmington, Delaware, USA). Kaolinite No. KGa-1 (Ward's Inc., Rochester, New York, USA) was used as a standard for kaolin loss between 450 and 550°C. Gibbsite loss near 300°C was compared to standard gibbsite No. C-730. Samples were heated from room temperature to 1000°C at a rate of 20°C per min under nitrogen.

2.1.4. Selective extractions

Analyses of total Fe in each of the size fractions were performed by digesting 0.1 g samples of each fraction in a teflon beaker with a solution consisting of 0.5 mL aqua regia and 3 mL HF (Thompson and Walsh, 1989). The suspensions were evaporated to dryness over a 12 h period, and residue was redissolved in 4 mL concentrated ultrapure HCl and diluted to 30 mL with water.

Free oxyhydroxides of Fe and associated Al were determined using the Ti(III)-citrate-EDTA-bicarbonate (TiCEB) method of Ryan and Gschwend (1991). Thirty mL of a 0.05 M Ti(III)-0.05 M citrate-0.05 M EDTA solution at pH 7.0 and 3.33 mL of 1 M HCO_3 were added to 0.1 g of each size fraction in 50 mL centrifuge tubes and shaken for 2 h with a wrist action shaker. The suspensions were centrifuged at 3400 g and a small amount (5 mL) of supernatant was carefully pipetted off for dilution and analysis. Several samples of the supernatant were also filtered with 0.02 μm syringe filters (Whatman Anotop) prior to dilution for comparison with unfiltered samples. All analyses for Fe and Al were performed using a Perkin Elmer model 4100ZL graphite furnace atomic absorption (A.A.) spectrometer. Standards were prepared with certified atomic absorption standards (Fisher Scientific).

Amorphous free oxyhydroxides of Fe and Al were determined using the ammonium oxalate (AOD) method (Schwertmann, 1964; Jackson et al., 1986). A 1 L solution, containing 567 mL of 0.2 M ammonium oxalate and 433 mL of 0.2 M oxalic acid, was brought to pH 3.0 with NaOH. Twenty five mL of this solution were added to 0.1 g of each size fraction in 50 mL centrifuge tubes. The tubes were immediately wrapped in aluminum foil to exclude light and were shaken for 2 h. The suspensions were centrifuged and a 5 mL aliquot of the supernatant was used for dilution and analysis of each sample.

Amorphous opaline silica was extracted with Tiron (4,5-dihydroxy-1,3-benzene disulfonic acid) using the method of Kodama and Ross (1991). One hundred twenty mL of a 0.09 M solution of Tiron, with 0.05 M Na_2CO_3 and 0.08 M NaOH added to buffer pH at 10.5, was added to 0.1 g of the <63 μm fraction. The samples were heated in a water bath at 80°C for 1 h. Subsamples were passed through 0.02 μm syringe filters and diluted for analysis by graphite furnace A. A. Peerless clay (South Carolina kaolin) (R. T. Vanderbilt Co., N.J.) was analyzed as a control to ensure that no kaolinite was being dissolved with the method.

2.1.5. Column Experiments to Mobilize Colloids

Column experiments, similar in design and function to those performed by Ryan and Gschwend, (1994), were conducted to mobilize inorganic colloids from the Georgetown sediment. Approximately 5 g of sediment were flushed with distilled water elevated to pH 9.0 with the addition of NaOH. Turbidity was monitored in line with a turbidimeter (Hach). Aqueous samples of the effluent were collected for AEM-TEM analysis.

2.2. Electron Microscopy

2.2.1. Sample preparation

Because the focus of this study was to observe undisturbed associations between the submicrometer grains in the sediment matrix, care was taken to maintain the natural state of the sediment in the

preparation of samples for AEM-TEM. To circumvent the need to desiccate our samples prior to embedding and to insure more adequate penetration of the embedding resin, Nanoplast® (Polysciences Inc.), was used. Because Nanoplast® is a water-soluble resin, there is no need to dry out the sample beforehand (Frösch and Westphal, 1989). Indeed, even aqueous samples have been directly embedded in the resin to view such phenomena as colloidal associations in lakewater samples (Perret et al., 1991; Leppard, 1993). The polymerization stage does involve a heating/desiccation step, but sample alteration due to dehydration and shrinkage is thought to be minimal due to the production of water during the polymerization process (Bachhuber and Frösch, 1983).

The resin was prepared using 1.0 g Nanoplast® and 0.0035 g hardener. This recipe was found to alleviate brittleness and fracturing without sacrificing strength. Two hundred μL of the resin was added by syringe to a compartment in a special mold (BEEM, Polysciences Inc.), and approximately 0.01 g of moist Georgetown sediment was taken from storage and placed in the resin. For colloidal samples released from the sediment, 50 μL of aqueous sample collected from column studies were immediately mixed with 150 μL of resin in the mold. The molds were then placed in a desiccator and the desiccator was placed in an oven set at 40°C for 48 h. Afterward, the molds were taken out of the desiccator and placed in the oven again, this time at 60°C for 48 h.

Ultramicrotomy was performed on trimmed faces of the samples using a DuPont Sorvar MT5000 Ultramicrotome at a speed of 0.5 mm/sec and a 45° diamond knife (Diatome). Fifty to seventy nm thick sections (thickness indicated by grey to silver color of thin sections in reflected light) were collected with 3 mm copper grids coated with formvar. Some of the grids were coated with a 0.10 nm thick carbon coating to prevent charging when under the electron beam.

2.2.2. *Microscopy*

Microtomed sections were examined using three electron microscopes. A JEOL 200CX, operating at 200 kV, was used for initial examination of all sections. The JEOL has a 0.24 nm point-to-point resolution and a coefficient of spherical aberration (C_s) of 1.2 mm. A Topcon 002B high resolution microscope (HRTEM) (200 kV, 0.18 nm point-to-point resolution, C_s = 0.4 mm) was used to obtain lattice fringe images of crystalline areas and to investigate crystalline/amorphous material associations in the sediment. Lattice spacings were calculated from lattice fringe counts measured directly from the high resolution electron micrographs with a Peak Anastigmat® micrograph viewer with a magnification of four times. Amorphous areas were recorded by focusing and stigmating the HRTEM on an area and quickly translating to a new area of specimen and obtaining micrographs within one minute or less to minimize radiation induced artifact. A VG HB603 scanning transmission electron microscope (STEM) (VG Microscopes, East Grinstead, UK), equipped with a energy dispersive x-ray (EDX) spectrometer (Link Analytical), was used to obtain elemental maps of selected areas in the sediment. The STEM was operated at 250 kV and has a 0.30 nm point-to-point resolution and a C_s = 4.5 mm. The beam width in the scanning mode is approximately 5.0 nm. Maps containing spatial distributions (as intensity per pixel) of selected elements (Si, Al, Fe) in the sections were obtained at a discretization of 128 by 128 pixels. The intensity data obtained from the EDX probe is directly proportional to the number of atoms of a particular element in the volume (probe area multiplied by the section thickness) analyzed. The EDX probe is operated with a 1 nm diameter. However, beam broadening caused by the thin section thickness expands the probe to a 2–4 nm diameter for a 50 nm thick sample (Garrett-Reed, 1995). Thus, the spatial resolution limit of a pixel in an EDX map is approximately 3 nm by 3 nm. Finally, a Cambridge Stereoscan 240 scanning electron microscope (SEM) equipped with an EDX spectrometer (Link Analytical) was used to study bulk sediment samples under low magnification. These samples were embedded in Spurrs® epoxy resin and sectioned with a diamond saw (Holmén, 1994).

Image analysis software (Aldus Photostyler 2.0) was used to colorize and superimpose elemental map files obtained from the VG STEM in order to elucidate spatial relationships among elements. Each element map was assigned a particular hue: green for Si; red for Al; and blue for Fe. Superposition of maps produces new colors if spatial comapping occurs among the elements. For example, yellow pixels will be produced if Si (green) and Al (red) comap, purple appears if Fe (blue) and Al comap, and white pixels occur if all three elements comap. Another software package (Image Pro Plus) was used to extract intensity data from specific areas of the element maps or along traverses across maps. The extracted data were used to calculate elemental mole ratios in the selected pixels using the appropriate Cliff-Lorimer (K) factors. These factors were experimentally determined with standards by the National Institute of Standards and Technology (Gaithersburg, Maryland, USA). Error introduced by not correcting for the particular history of the spectrometer attached to the HB603 is expected to be ≤5% (Bell, 1996).

3. RESULTS AND DISCUSSION

3.1. Sediment Characterization

The sediment is composed predominantly of medium to fine sand (Table 1). The <63 μm fraction is 12% by weight of the sediment, and the clay-size (<2 μm) material makes up approximately 2.5% by weight of the sediment. The <63 μm fraction has a low organic carbon content, typically only 0.6% by weight (Holmén, 1994).

The mineralogy of the sediment is dominated by quartz, with minor amounts of feldspar and mica in the sand- and silt-size fractions. Ilmenite ($FeTiO_3$) and rutile (TiO_2) are the chief heavy minerals present and are present mostly in the fine sand- to silt-size fractions (Table 1). Finely divided iron oxyhydroxides and clay minerals fill the interstitial voids between sand-size grains. Readily detected minerals include goethite (α-FeOOH), kaolinite, gibbsite ($Al(OH)_3$), quartz, and vermiculite in the <2 μm fraction (Fig. 1). Minor components such as lepidocrocite (γ-FeOOH) may also be present, as suggested by the small peak at 14° 2θ (6.3 Å d spacing; Fig. 1). Kaolinite is the largest component of the clay-size fraction (40–45% by weight), typical for sediments in the Southeastern Coastal Plain (Dixon, 1989). Gibbsite constitutes approximately 4–8% of the <2 μm fraction. The measured Al concentrations ($9.3 \times 10^{-8} \pm 4.6 \times 10^{-8}$ M) in groundwater at the site were indistinguishable from expectations assuming gibbsite dissolution equilibrium (7.9×10^{-8} M), calculated using a solubility constant (K_s) equal to $10^{-33.5}$ and a pH of 5.2 (Morel and Hering, 1993).

Most of the Fe in every size fraction comprises Fe incorporated in iron oxyhydroxides, the largest amount of Fe being in the <63 μm fraction (Table 1). The small amounts of TiCEB-extractable Fe in the larger size fractions probably represent iron oxyhydroxide coatings which were not entirely removed from the quartz grains during wet sieving. The total TiCEB-extractable Fe (1250 μmol g^{-1}, Table 1), minus the amount of AOD-extractable Fe (64 μmol g^{-1}, or 5% of TiCEB-extractable Fe, Table 1), equals the amount of Fe incorporated in crystalline iron oxyhydroxides (1190 μmol g^{-1}). To calculate the weight percent crystalline iron oxyhydroxides in the <63 μm fraction, the chemical formula FeOOH (representing goethite and lepidocrocite) was used. On this basis, crystalline iron oxyhydroxides make up approximately 10% by weight of the <63 μm fraction of the Georgetown sediment.

TABLE 1. Distribution of grain size fractions, heavy minerals, and Fe and Al associated with free oxyhydroxide phases

Size Fraction (μm)	wt. %	Heavy Min. wt. %	Total Fe (μmol/g)[a]	TICEB Fe (μmol/g)[b]	AOD Fe (μmol/g)[c]	TICEB Al (μmol/g)[b]
Bulk		na[e]	180 (15)[d]	180 (7)	18 (1)	40 (28)
>1000	5	na	na	13 (9)	<1	<1
1000-500	18	na	8.8 (1.8)	9 (2)	<1	<1
500-250	26	<0.1	9.3 (0.8)	11 (8)	<1	<1
250-125	38	0.3	9.3 (0.3)	14 (4)	1.4 (1)	<1
125-63	1	6	440 (17)	99 (36)	12 (2)	18 (10)
<63	12	2	1360 (95)	1250 (166)	64 (2)	320 (30)

[a]Determined by digestion with HF-HCl-HNO_3 (Thompson and Walsh, 1989)
[b]Determined by Ti-Citrate-EDTA-HCO_3 method (TiCEB) (Ryan and Gschwend, 1991)
[c]Determined by ammonium oxalate method (AOD) (Jackson, et al., 1986)
[d]One standard deviation, based on 3 replicates, enclosed in parentheses
[e]not analyzed

The values for TiCEB-extractable Fe and total Fe in the <63 μm fraction were nearly the same (Table 1), although the slightly larger amount of total Fe could have included some structural Fe released from heavy minerals (e.g., ilmenite) and Fe-substituted kaolinite. Heavy mineral content was highest in the 125–63 μm fraction, coinciding with a total Fe content that was over four times more than the TiCEB-extractable Fe (Table 1).

TiCEB-extractable Al was small in each of the fractions except for the <63 μm fraction (320 μmol g^{-1}, Table 1). AOD-extractable Al was measurable only in the <63 μm fraction (46 ± 2 μmol g^{-1}, data not shown in Table 1). Data presented below (see section 3.2.3) indicate that most of the TiCEB- and AOD-extractable Al was associated with the goethite and amorphous iron oxyhydroxides, respectively.

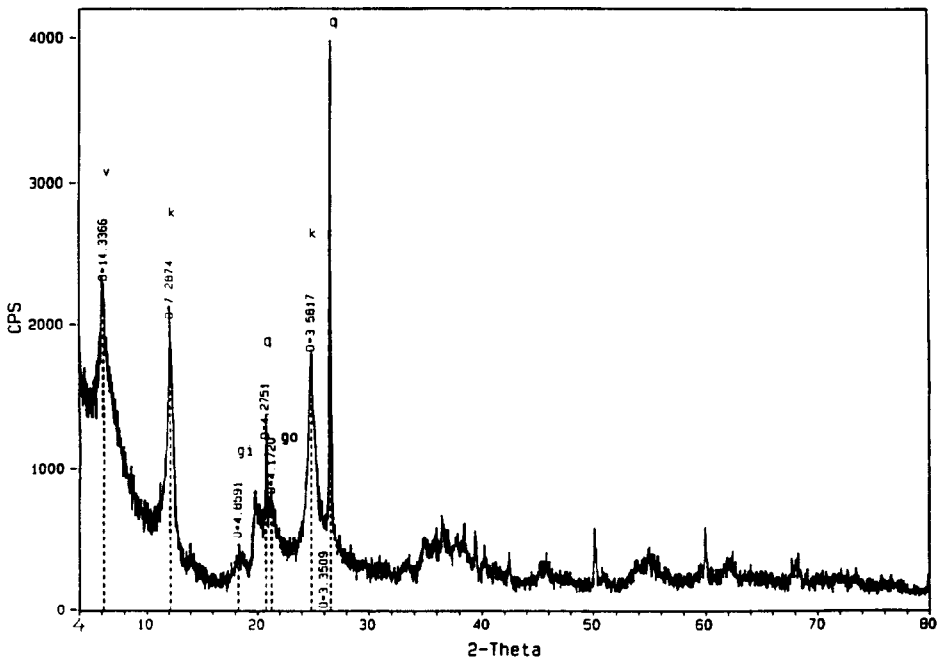

Fig. 1. XRD pattern of the <2 μm size fraction of the Georgetown sediment. v = vermiculite, k = kaolinite, gi = gibbsite, go = goethite, q = quartz.

Fig. 2. SEM backscatter image of the mineral material filling the interstitial matrix (marked M) between approximately 200 μm diameter quartz grains and smaller quartz fragments (marked Q). The scale bar represents 100 μm.

3.2. Electron Microscopy

3.2.1. General Morphology

The silt- and clay-size mineral materials fill the voids between the sand-size quartz grains in the Georgetown sediment (Fig. 2). The roughly 200 μm diameter quartz grains were separated by spaces filled with mineral particles too small to be resolved at this magnification. Also, fragments of quartz, tens of micrometers in diameter, were incorporated in the interstitial matrix. It is the nanometer-scale associations among these mineral materials that we investigated using AEM-TEM. SEM-EDX analysis of the matrix indicated the presence of abundant Si, Al, and Fe, as expected for a kaolinite- and goethite-rich matrix.

3.2.2. Clay Mineral Arrangement

The clay minerals (kaolinite, vermiculite) present in the Georgetown sediment made up the majority by weight of the <63 μm fraction. In the Georgetown matrix, stacked assemblages, or books, of face-associated kaolinite particles, tens of nanometers thick and up to 100–200 nm long, were prevalent (Fig. 3, point a). These books were assembled in domains up to several micrometers wide and several micrometers long, extending through the matrix in a chain-like manner. This type of clay particle arrangement has been observed in other undisturbed sediments (Collins and McGown, 1974; Bennett et al., 1981).

Edge-face contacts represented boundaries where domains of clay books were rotated at right angles or obliquely to the domains observed on edge (Fig. 3, point c and marked with arrows). It was difficult to discern individual particles in these domains due to the low contrast these areas exhibited (Fig. 3, point d). Also, possible intergrowth among particles has been observed in other sediments and could contribute to difficulty in identification of book boundaries (Collins and McGown, 1974). Voids, 50 nm or less in diameter, which appear within these domains, were suspected to be undisturbed pore spaces representative of the matrix (Fig. 3, point e). The separations between some books in our samples (see Fig. 3, point b) may be due to tearing that occurred as a result of the microtoming process (Smart and Tovey, 1981).

3.2.3. Iron Character and Distribution

Crystalline Iron. Iron-rich zones in thin sections of the Georgetown matrix were easily observed in the TEM due to the stronger contrast and morphological differences they exhibited vs. the clays around them. These iron-rich aggregates were typically subcircular in profile and approximately 500 nm in diameter, as can be seen in the Si, Al, and Fe composite STEM-EDX map of a representative aggregate (Fig. 4). Higher magnification revealed that these iron-rich zones were composed of spheroidal subunits, approximately 5–10 nm in diameter, and analysis of electron diffraction patterns taken from these areas confirmed the presence of polycrystalline goethite. In addition, lattice fringe images with spacings 4.2 Å apart, representing the [110] lattice plane spacing of goethite (4.17 Å spacing), were recorded in these aggregates (Fig. 5, subhorizontally oriented set of fringes). The subvertically oriented set of lattice fringes, spaced 3.6 Å apart, probably represents the [120] lattice

Fig. 3. TEM image of clay associations in the Georgetown matrix. Points marked as the following: (a) kaolinite book with face-face contacts, (b) void possibly created by ultramicrotome tearing, (c) edge-face contact with boundary marked by arrows, (d) books oriented with faces at right angles or obliquely to the image plane, (e) suspected naturally occurring void space. The scale bar represents 270 nm.

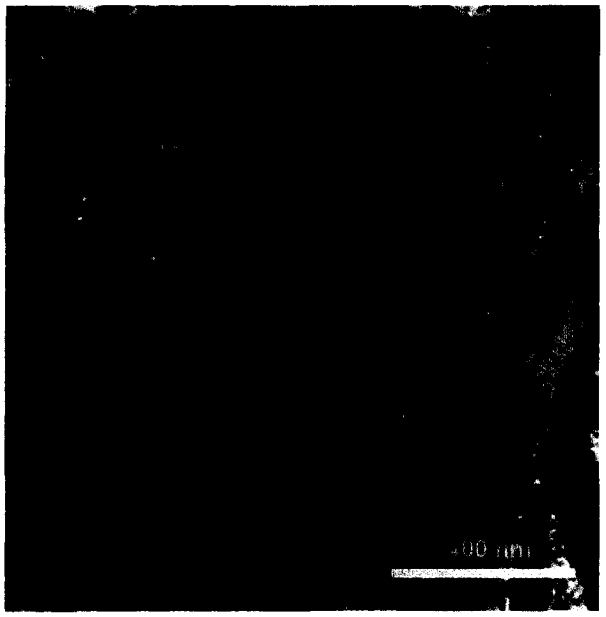

Fig. 4. STEM-EDX Si, Al, and Fe composite map of a representative goethite aggregate. Green pixels indicate presence of Si; red, Al; and blue, Fe. Yellow pixels indicate comapping of Si and Al and represent the clay minerals. Purple pixels indicate association of Al with the goethite. The red particle is probably gibbsite ($Al(OH)_3$). The scale bar represents 400 nm. Each pixel represents approximately 12 × 12 nm of sample area.

spacing of goethite (3.38 Å) observed at an angle to the electron optical axis or perhaps the [002] lattice spacing of kaolinite (3.57 Å) underlying the goethite (Fig. 5). However, an electron diffraction pattern was not recorded for this particular area of the specimen to determine which mineral was represented by the 3.6 Å spaced lattice fringes. All of the goethite aggregates observed in the matrix were relatively isolated and were separated by hundreds of nanometers from each other so that only approximately ten aggregates were found per 100 μm^2 of matrix.

A significant amount of Al was found to be associated with the goethite aggregates (Fig. 4). The mole fraction of Al/Fe, calculated using Al and Fe intensity data within the boundaries of the goethite aggregates, was found to be 0.24 ± 0.08 (n = five aggregates). This Al/Fe mole ratio corresponds very well to that calculated (0.23 Al/Fe) using the amount of TiCEB-extractable Al for the <63 fraction (320 μmol g^{-1}, Table 1) minus the AOD-extractable Al (46 μmol g^{-1}). The calculations assume the total TiCEB-extractable Al, less the AOD-extractable Al, is associated with the Fe (1190 μmol g^{-1}) in goethite.

Amorphous Iron. In contrast to the Fe signal representing the goethite aggregates, we also detected a population of Fe dispersed relatively homogeneously throughout the clay-dominated matrix (Fig. 6). This population of Fe consisted predominantly of particles on the order of, or less than, the pixel size (12 nm) of Fig. 6 (examples marked a). Higher magnification STEM-EDX Si, Al, and Fe composite maps indicated that much of this Fe was directly associated with the surfaces of individual clay particles (Fig. 7). It appeared that the Fe (Fig. 7, blue to purple, marked Fe) was present as approximately a 10 nm thick medium positioned between the faces of two clay books (Fig. 7, yellow, marked K). Some larger, more discrete particles, or aggregates of particles, tens of nanometers in diameter, were also represented by the dispersed Fe signal (Fig. 6, examples marked b).

We believe this dispersed Fe signal represents much of the AOD-extractable Fe (64 μmol g^{-1}) in the <63 μm fraction. This Fe may be present as amorphous iron oxyhydroxides, Fe ions, and/or Fe polymers on the clay mineral surfaces. The Al/Fe mole ratio for portions of this dispersed Fe phase was found to be 0.44 ± 0.14 (n = ten particles) using Al and Fe intensity data from the centers of particles large enough to observe discernable boundaries (i.e., particles such as those marked b in Fig. 6). This ratio is lower than the Al/Fe mole ratio (0.72) calculated using the AOD-extractable Al (46 μmol g^{-1}) and Fe (64 μmol g^{-1}) data for the <63 μm fraction, possibly due to the bias of sampling only the larger particles. However, this ratio is much higher than the Al/Fe mole ratio calculated for the crystalline iron oxyhydroxides (0.23, see section on crystalline iron above), and supports our interpretation that the homogeneously dispersed Fe signal mostly represents the AOD-extractable Fe phases.

A portion of the homogeneously dispersed Fe signal could

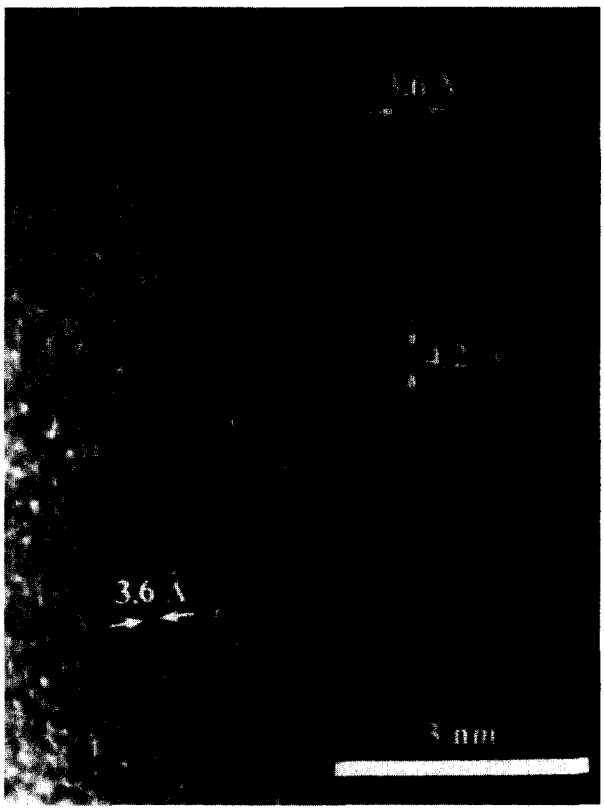

Fig. 5. HRTEM lattice fringe image of goethite. The subhorizontally oriented fringes have spacings 4.2 Å apart and indicate the [110] lattice planes of goethite. The subvertically oriented fringes spaced 3.6 Å apart possibly represent the [120] lattice spacing of goethite (3.38 Å) or the [002] lattice planes of kaolinite (3.57 Å), which underlies the goethite. The scale bar represents 3 nm. Magnification is 6,500,000×.

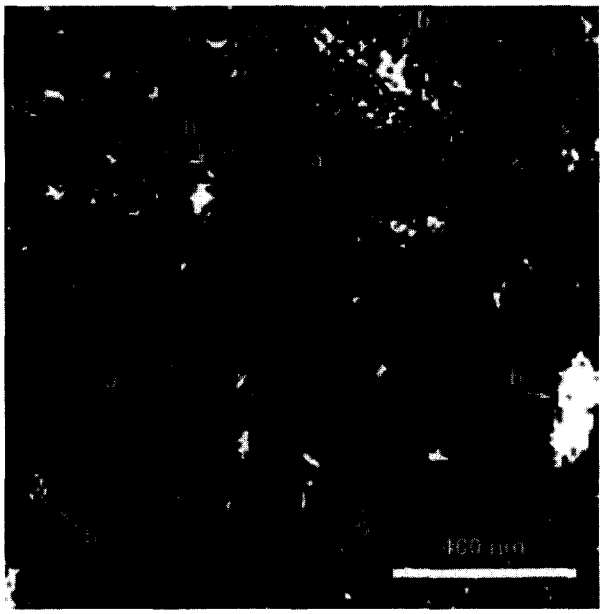

Fig. 6. STEM-EDX map of iron distributed among the clay particles. The fainter population of pixels (marked a) represent amorphous iron oxyhydroxides, adsorbed Fe, and possibly structural Fe in the clays at the scale of approximately 12 nm or less (the sample area represented by each pixel), whereas the particles marked b likely represent larger particles of amorphous iron oxyhydroxide tens of nanometers in diameter. The scale bar represents 400 nm.

represent Fe in the structure of kaolinite and vermiculite as well. Structural Fe in kaolinite from South Carolina sediments has been found to be approximately 1.0% by weight (Jefferson et al., 1975). As the percent by weight of kaolinite in the Georgetown <2 μm size fraction is at least 40%, the amount of structural Fe present in the <2 μm fraction, therefore, could be approximately 0.4% by weight. Such structural Fe would probably be represented by discrete Fe signals 3 nm or less in dimension and would be indistinguishable from simple adsorbed Fe or discrete Fe polymers in the STEM-EDX maps.

3.2.4. Evidence for an Amorphous, Siliceous Phase

Observation of sample sections under HRTEM revealed areas among the clay domains which appeared amorphous in nature (Fig. 8). Lattice fringes, spaced 2.5 Å apart, appear in the central portion of the image (Fig. 8) and likely correspond to the [200] (2.50 Å) or the [130] (2.54 Å) lattice plane spacing of kaolinite. A phase lacking periodicity surrounds these fringes. These amorphous areas appeared to be too large and continuous to be attributed entirely to the dispersed amorphous Fe phase. They lacked the contrast of the Fe-rich phase as well.

STEM-EDX evidence suggested that a siliceous phase was responsible for these amorphous areas, as an excess of Si was observed in parts of the matrix (Fig. 9a). Of the one hundred and twenty-eight data points from this representative traverse across a distance of approximately 1.5 μm in the matrix, 25% indicated essentially infinite Si/Al ratios (points along the y axis of Fig. 9a). Spatially, these Si-enriched areas corresponded to dimensions several tens of nanometers wide in the mapped traverses. Other points fell along a line representing a 1:1 Si/Al ratio and indicated the presence of kaolinite (Fig. 9a). The points which fell on the x axis represented Si-lacking phases and probably corresponded to Al incorporated in the dispersed amorphous Fe phase or gibbsite particles. The points representing voids (intensity values of zero for both Si and Al) were not plotted. When data from traverses across other areas of matrix were plotted, Si/Al ratios fluctuated closely about the 1:1 ratio expected for kaolinite (Fig. 9b). The average Si/Al ratio was 1.2 $\pm$ 0.5 for this 1.5 μm traverse. The few points representing Si/Al ratios of 2:1 to 3:1 possibly indicated interspersed vermiculite, as Si/Al ratios in the range of 1.5:1 to 5.6:1 are commonly observed in the relatively unweathered vermiculite identified by XRD in this sediment (Douglas, 1989).

Confusion with quartz can not explain the infinite Si/Al ratios observed, as quartz grains observed in sections were microscopically obvious at approximately 1–2 μm and were too large to contribute to the ubiquitous Si that mapped with dimensions on the order of tens of nanometers in these areas. Possible silica contamination due to grinding of quartz grains during ultramicrotoming was ruled out, as EDX analysis of the Nanoplast® near the boundaries of the matrix revealed very little background Si.

A hydrous alumino-silicate exhibiting no long range order would produce an electron amorphous coating if associated with the kaolinite and vermiculite in the matrix. Allophanic materials, however, are considered AOD-extractable (Wada, 1989). Only 46 μmol g^{-1} Al (0.1% by weight) were ex-

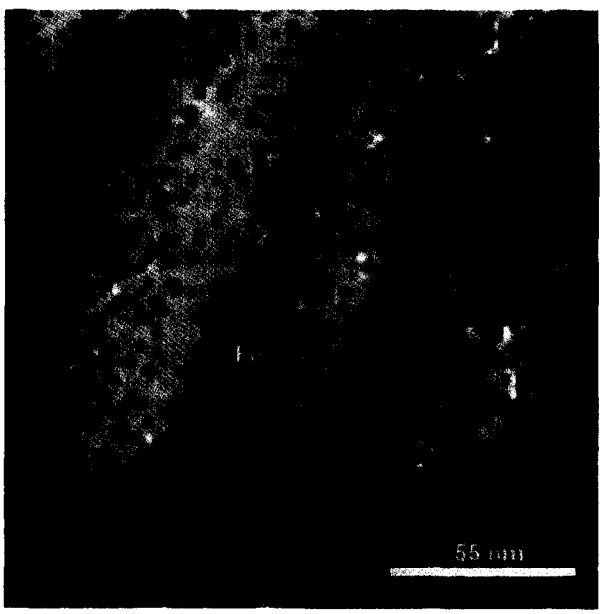

Fig. 7. STEM-EDX Si, Al, and Fe composite map of the associations between the dispersed, amorphous iron oxyhydroxide phase (marked Fe) and kaolinite particles (marked K). The 10 nm thick iron phase (blue) lies between two clay books (yellow). The scale bar represents 55 nm. Each pixel represents approximately 3 × 3 nm of sample area.

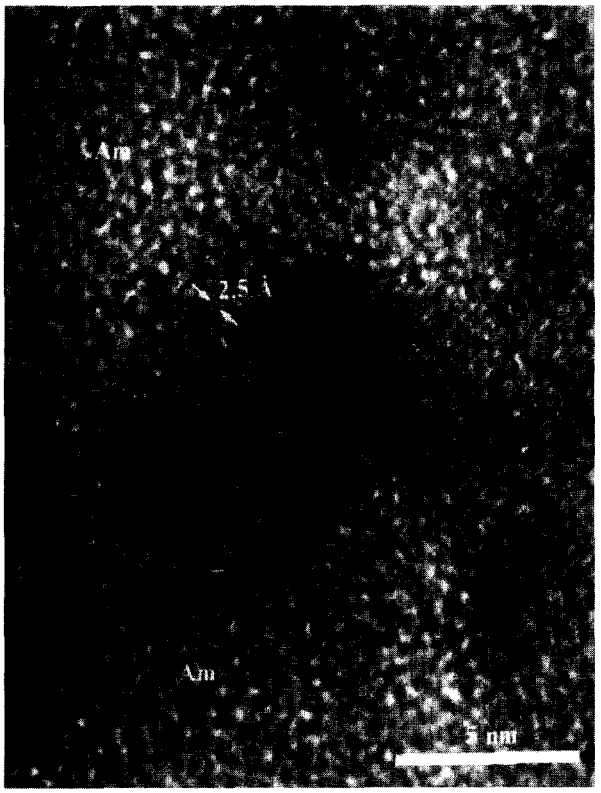

Fig. 8. HRTEM image of a crystalline phase associated with an amorphous phase. Lattice fringes spaced 2.5 Å apart possibly represent the [200] (2.50 Å) or the [130] (2.54 Å) lattice plane spacing of kaolinite. The fringes are surrounded or partially coated by an amorphous phase (marked Am). The scale bar represents 5 nm. Magnification is 4,970,000×.

tracted from the <63 μm fraction, and this Al appeared, in large part, to be associated with the AOD-extractable Fe phase (see section 3.2.3).

We suggest that the phase represented by the infinite Si/Al ratios is a form of opaline silica, probably of biogenic origin. Biogenic opal has no long range order and is a common constituent in forested soils, as it is a product of plant processes (Wilding and Drees, 1973; Wilding et al., 1979; Drees et al., 1989). Because the Georgetown sediment samples were recovered from the C horizon of a heavily forested soil, it is reasonable to conclude that an opaline silica phase is responsible, at least in part, for the amorphous character of portions of the matrix observed under HRTEM. Siliceous, cementitious coatings on and between clay particles have been observed previously in sediment and shale samples using AEM-TEM (Lee et al., 1991; Banfield et al., 1991). Tiron extraction of the <63 μm fraction revealed $1.2 \times 10^{-3} \pm 6.2 \times 10^{-4}$ moles Si g^{-1} (based on three replicates), indicating that opaline silica constituted approximately 10% by weight of this size fraction. This calculation assumes the opal contains 18% by weight water (Kodama and Ross, 1991). In addition, groundwater composition data support the conclusion that this Si phase is opal, as dissolved Si concentrations were found to be 14 ± 2 ppm for samples from three different wells screened near the depth at which the sediment sample was collected. The solubility of opal can range from 0.5 to 10 ppm, depending on the amount of adsorbed Fe and Al (Wilding et al., 1979; Bartoli and Wilding, 1980).

3.3. Implications for Colloid Mobilization

From the associations observed among the clay minerals, the iron oxyhydroxide phases, and the siliceous phase in the STEM-EDX and TEM/HRTEM images, some general hypotheses of the binding forces acting in the Georgetown matrix can be constructed. Electrostatic interactions can help to explain the edge-face associations observed among the clay books (Fig. 3). The interparticle associations among kaolinite books could be controlled by the differences in surface charge between the edges, which have a variable charge dependent on pH, and the faces, which have a constant negative charge (van Olphen, 1977; Newman and Hayes, 1990). Because the pH_{pzc} of kaolinite edges occurs

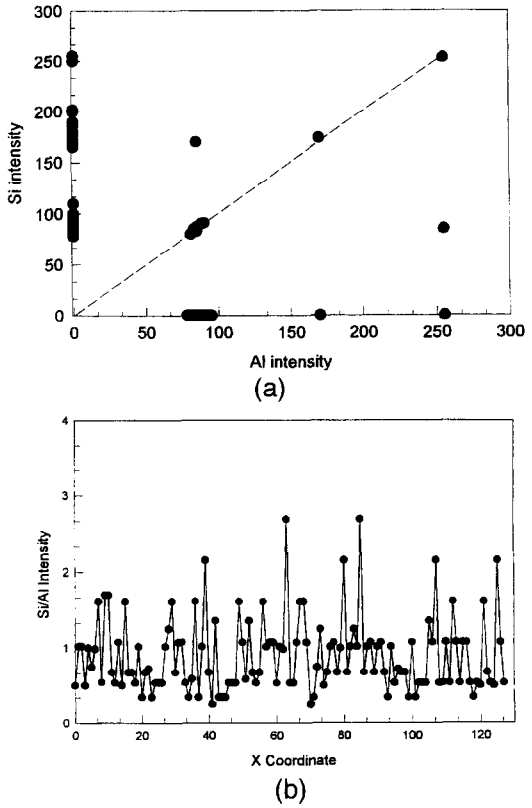

Fig. 9. Variation in Si and Al in two different traverses across matrix. (a) Si is plotted vs. Al for the first traverse of 1.5 μm. Three different populations of points are present. Points falling along the y axis indicate a siliceous phase with essentially infinite Si/Al ratios. Points falling along the dashed line representing a 1:1 Si/Al ratio indicate kaolinite. Points along the x axis indicate Si-lacking phases, probably the dispersed, amorphous Fe-Al phase, or gibbsite. (b) Si/Al ratio is plotted against the x coordinate for the second 1.5 μm traverse. The majority of points oscillate around a mean Si/Al ratio of 1.2 ± 0.5, and indicate kaolinite particles. Si/Al ratios of 2:1 to 3:1 possibly represent vermiculite. For each plot, each data point represents intensity data taken from an area of approximately 12 × 12 nm in the samples.

around a pH of 7.0 (Herrington et al., 1992), the faces and edges of kaolinite plates can possess opposite charge. In theory, electrostatic considerations would dictate a card house structure in which individual clay plates are associated face-to-edge to limit electrostatic repulsion (van Olphen, 1977). In the Georgetown sediment, these edge-face associations are observed among the aggregates of clay platelets, or books. High electrolyte concentration diminishes double layer repulsive forces among clay platelets so that attractive van der Waals forces can allow the similarly charged surfaces of the clays to assemble in the domains of face-associated books observed in the Georgetown sediment (Fig. 3; Collins and McGown, 1974; Yariv and Cross, 1979). Because the Georgetown sediment was deposited in a marine beach environment, it is likely that saline or brackish pore fluids promoted this arrangement as the clays were emplaced after sand deposition and winnowing. Most kaolinite in the southeastern Coastal plain sediments is thought to be inherited (Dixon, 1989).

Aggregation of the clay books could be promoted by the presence of a net positively charged phase or specific sorbate which serves as an electrostatic intermediary and diminishes repulsive forces among the faces of juxtaposed clay booklets. It is also possible that the intermediary could promote aggregation among the clay books through the creation of bonds between itself and the surface functional groups of the clay books. In either case, the distribution of this phase among the clay books would be an important factor in its ability to act as a binding agent and hold the fines together. The TEM and STEM-EDX data presented above indicate that the goethite phase is manifested in the Georgetown sediment as discrete, isolated aggregates (Fig. 4). This distribution pattern, observed in the clay fractions of some tropical soils as well (Greenland et al., 1968; Jones et al., 1982; Schwertmann and Kampf, 1985), renders goethite ineffective as a binding agent in the Georgetown sediment even though it is approximately 10% by weight of the <63 μm size fraction and makes up 95% of TiCEB-extractable Fe. Indeed, Deshpande et al. (1968) found that removal of the majority of the free iron oxyhydroxides thought to occur as discrete particles in a variety of soils had little effect on the aggregative properties of the soils. In contrast, it appears that the AOD-extractable, amorphous iron oxyhydroxide phase (Fig. 6), which represents only 5% of TiCEB-extractable Fe, serves as an intermediary among the clay books (Fig. 7). Although this dispersed Fe phase is only 0.4% by weight of the <63 μm size fraction, minor amounts (0.1–1% by weight) of iron polycation phases have been shown to promote effectively aggregation among fine-grained clay particles (Oades, 1984). In addition, Fe phases of low crystallinity have been shown to be more effective at aggregating soil fines than crystalline phases such as goethite and hematite (Schahabi and Schwertmann, 1970). Iron phases of lower crystallinity are more effective at aggregation probably due to their more reactive surface areas, which can be as much as ten times larger than the surface area of goethite (Schindler and Stumm, 1987; Schwertmann and Taylor, 1989).

Thus, the iron oxyhydroxide phase associations observed in the Georgetown sediment might be typical of a variety of sediments comparable in mineralogy and weathering history.

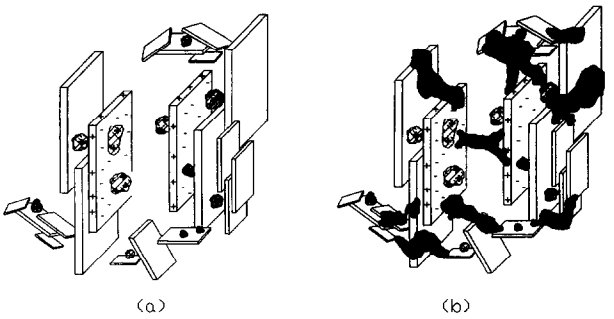

Fig. 10. Schematic diagram of the nanometer-scale associations among mineral particles in the Georgetown matrix. (a) an amorphous iron oxyhydroxide phase (hatched) could act as an electrostatic or bonding intermediary between kaolinite books. Positive charge (dispersed Fe phase and the edges of kaolinite books) and negative charge (faces of kaolinite books) are partially represented. (b) Opaline silica (solid) could act as a cemetitious phase, incorporating micrometer-scale aggregates of associated clay and iron oxyhydroxide particles in a web-like encasement. Partial dissolution may be required to release the clay and iron oxyhydroxide particles within.

The importance of correctly assigning the function of intermediary predominantly to that of the amorphous Fe phase, rather than to a crystalline phase such as goethite, lies in consideration of the differing pH_{pzc}'s, solubilities, and site densities of the two phases. By assuming goethite to be the active intermediary, one would incorrectly estimate the amount of surface-active solute needed to reverse surface charge or the amount of iron oxyhydroxide needed to be dissolved in order to induce mobilization of mineral colloids.

The AEM-TEM data suggest that at least two components serve to bind the Georgetown matrix (Fig. 10). The homogeneously dispersed, amorphous Fe phase might operate as an intermediary among the clay books, as discussed above. This amorphous Fe phase might reduce repulsive electrostatic interactions among the clay books by serving as a net positively charged intermediary (Fig. 10a). The positioning of the amorphous Fe phase between the faces of the kaolinite books in Fig. 7 supports the possibility that at least some of amorphous Fe-clay book associations are electrostatic in origin. It is also possible that bonds exist between the amorphous Fe phase and surfaces (edges) of clay books. The AEM-TEM data, however, can not be used to differentiate between these types of binding mechanisms.

The presence of an amorphous siliceous phase in the Georgetown matrix suggests another possible component involved in binding the matrix fines. The opaline silica might mechanically bind the clay aggregates in a web-like cage (Fig. 10b). It is also possible that opaline silica might possess bond linkages with the clay books in a manner similar to that suggested for the amorphous Fe phase. Finally, the opaline silica phase might be electrostatically associated with the clay minerals, especially the clay edges, and the iron oxyhydroxides. In this respect, the opaline silica would be just another participant in the overall electrostatic balance holding the matrix material intact.

If these components have a significant role in holding the Georgetown matrix together, evidence of their roles may

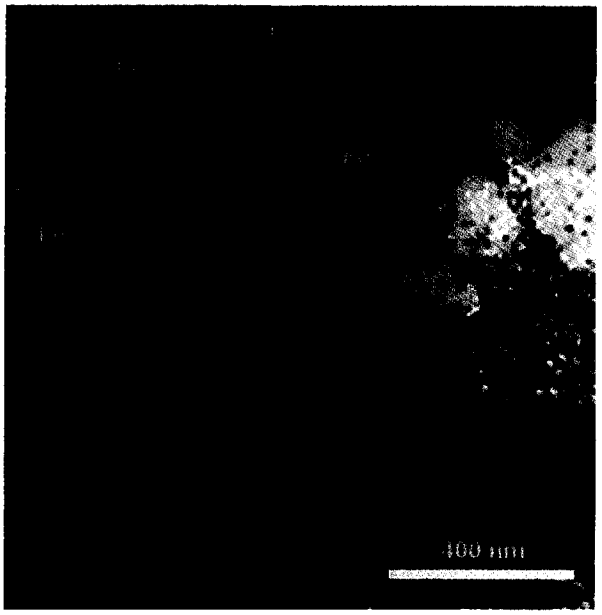

Fig. 11. Associations among colloids released from the Georgetown sediment at pH 8.4 represented in a STEM-EDX Si, Al, and Fe composite map of a sample of embedded and ultramicrotomed colloids. Note the ubiquity of green pixels, indicating the abundance of a Si-rich phase. Clay particles (yellow) appear to be incorporated in the Si phase (indicated with arrows). The white and blue pixels in this area of the image represent an Fe-rich particle situated above the clay/Si aggregate. Some discrete iron oxyhydroxide particles (marked Fe) appear to be no longer specifically associated with the clays. The scale bar represents 400 nm. Each pixel represents approximately 12 × 12 nm of sample area.

be observable in particle associations among the colloids released from the sediment (Fig. 11). The most obvious feature of this STEM-EDX map of colloids mobilized from the Georgetown sediment at pH 8.4 is the abundance of green pixels, indicating a large amount of siliceous material in this sample of column effluent (Fig. 11). Much of this siliceous material occurred in large (tens of nanometers) clumps or aggregates. In TEM, this siliceous material appeared crust-like or web-like in nature, suggesting that this material encrusted or mechanically bound clay particle aggregates. Indeed, we observed such Si-encapsulated material in the STEM-EDX map (Fig. 11, clay particles in yellow). The structures did not appear to be the result of the embedding process, as embedded aqueous samples of 1–1000 μM Si standards yielded Si maps with this element homogeneously distributed and unaggregated when analyzed by STEM-EDX. Note also that Fig. 11 contains an amount of Si that does not correspond, in mass balance terms, to the amount of opaline Si extracted from the <63 μm fraction, as the image was recorded in a very Si-rich portion of a thin section of the column effluent where the Si-enriched structures were most microscopically apparent. Small iron oxyhydroxide particles (blue, marked Fe) mostly did not appear to be associated with the clay particles (Fig. 11), indicating that at least some of the iron oxyhydroxide-clay particles associations observed in the undisturbed matrix had been altered by mobilization. Thus, these observations appear to implicate the opaline silica phase in a role as binding agent, possibly in tandem with the amorphous Fe phase, in the Georgetown matrix.

4. CONCLUSION

Nanometer-scale spatial associations among clay-sized mineral particles in the matrix of an aquifer sediment were observed via TEM/HRTEM and STEM-EDX. Clay minerals were found to aggregate in face-associated domains. Two distinct populations of iron oxyhydroxide phases were observed, supporting data derived from wet chemical, selective-extraction analysis of the sediment. A crystalline phase (goethite) was self-associative and thus unable to play a role in matrix binding. A second phase, probably composed of amorphous iron oxyhydroxide and adsorbed Fe and/or iron polymers, was found to be distributed homogeneously throughout the matrix. It is this dispersed Fe phase that should be the effective binding intermediary among the clay books. Furthermore, a siliceous phase, likely biogenic opal, was observed in the matrix and in colloid samples released from the sediment. The presence of this siliceous phase suggests that mechanical entrapment of colloids may inhibit their release. Thus, dissolution processes might play a role in mobilizing colloids in this aquifer.

Acknowledgments—Mike Frongillo and Anthony Garrett-Reed (electron microscopy facility, Center for Materials Science, MIT) provided instruction on use of the Jeol 200CX and HB603 VG-STEM and Pat Reilly (electron microscopy facility, Dept. of Biology, MIT) provided ultramicrotome instruction. Mike Frongillo also obtained the HRTEM micrographs. Stacy Kirsch, Electron Microscopy Sciences, Warrenton, PA, gave advice on diamond blade use and provided us with initial thin sections of the Georgetown sediment. John MacFarlane, John McCarthy, Jim Morris, and Tom Williams helped with sediment coring at Georgetown and Lou Jolley performed the major cation and anion chemistry of the groundwater. We gratefully acknowledge the insights received on this research from Britt Holmén and Bill Casey at U.C. Davis, and Bob Graham and Kathy Tice at U.C. Riverside. We also thank P. Cambier and G. Vrdoljak for their helpful reviews of this paper. This research was supported by Dr. Frank Wobber, Subsurface Science Program, US Department of Energy, under contract DE-FG02-89ER60846 and by the National Science Foundation under contract CTS-9523824. Such support does not constitute an endorsement by D.O.E. or N.S.F. of the views expressed in this article.

Editorial handling: G. Sposito

References

Bachhuber K. and Frösch D. (1983) Melamine resins, a new class of water-soluble embedding media for electron microscopy. *J. Microsc.* **130,** 1–9.

Backhus D. A., Ryan J. N., Groher D. M., MacFarlane J. K., and Gschwend P. M. (1993) Sampling colloids and colloid associated contaminants in groundwater. *Groundwater* **31,** 466–479.

Banfield J. F., Jones B. F., and Veblen D. R. (1991) An AEM-TEM study of weathering and diagenesis, Abert Lake, Oregon. *Geochim. Cosmochim. Acta* **55,** 2781–2793.

Bartoli F. and Wilding L. P. (1980) Dissolution of biogenic opal as a function of its physical and chemical properties. *Soil Sci. Soc. Amer. J.* **44,** 873–878.

Bennett R. H., Bryant W. R., and Keller G. H. (1981) Clay fabric of selected submarine sediments: Fundamental properties and models. *J. Sediment Petrol.* **51,** 217–232.

Buddemeier R. W. and Hunt J. R. (1988) Transport of colloidal

contaminants in groundwater: Radionuclide migration at the Nevada test site. *Appl. Geochem.* **3,** 535–548.

Cerda C. M. (1987) Mobilization of kaolinite fines in porous media. *Coll. Surf.* **27,** 219–241.

Collins K. and McGown A. (1974) The form and function of microfabric features in a variety of natural soils. *Geotechnique* **24,** 223–254.

Degueldre C., Baeyans B., Goerlich W., Riga J., Verbist J., and Stadelmann P. (1989) Colloids in water from a subsurface fracture in granitic rock, Grimsel test site, Switzerland. *Geochim. Cosmochim. Acta* **53,** 603–610.

Deshpande T. L., Greenland D. J., and Quirk J. P. (1968) Changes in soil properties associated with the removal of iron and aluminum oxides. *J. Soil Sci.* **19,** 123–126.

Dixon J. B. (1989) Kaolin and serpentine group minerals. In *Minerals in Soil Environments* (ed. J. B. Dixon and S. B. Weed), 2nd ed., pp. 467–526. Soil Sci. Soc. Amer.

Douglas L. A. (1989) Vermiculites. In *Minerals in Soil Environments* (ed. J. B. Dixon and S. B. Weed), 2nd ed., pp. 635–674. Soil Sci. Soc. Amer.

Drees L. R., Wilding L. P., Smeck N. E., and Senyaki A. L. (1989) Silica in soils: Quartz and disordered silica polymorphs. In *Minerals in Soil Environments* (ed. J. B. Dixon and S. B. Weed), 2nd ed., pp. 913–974. Soil Sci. Soc. Amer.

Frösch D. and Westphal C. (1989) Melamine resins and their application in electron microscopy. *Elec. Micr. Rev.* **2,** 231–255.

Gee G. W. and Bauder J. W. (1986) Particle size analysis. In *Methods in Soil Analysis. Part 1-Physical and Mineralogical Methods* (ed. A. Klute), pp. 383–411. Amer. Soc. Agron. Inc.

Greenland D. J., Oades J. M., and Sherwin T. W. (1968) Electron microscopic observations of iron oxides in some red soils. *J. Soil Sci.* **19,** 123–126.

Gschwend P. M., Backhus D. A., MacFarlane J. K., and Page A. L. (1990) Mobilization of colloids in groundwater due to infiltration of water at a coal ash disposal site. *J. Contam. Hydrol.* **6,** 307–320.

Gschwend P. M. and Reynolds M. D. (1987) Monodisperse ferrous phosphate colloids in an anoxic groundwater plume. *J. Contam. Hydrol.* **1,** 309–327.

Hendershot W. H. and Lavkulich L. M. (1983) Effect of sesquioxide coatings on surface charge of standard mineral and soil samples. *Soil Sci. Soc. Amer. J.* **57,** 1252–1260.

Herrington T. M., Clarke A. Q., and Watts J. C. (1992) The surface charge of kaolin. *Coll. Surf.* **68,** 161–169.

Holmén B. A. (1994) Polycyclic Aromatic Hydrocarbon Sorption Kinetics in Three Aquifer Sands. PhD. dissertation, Massachusetts Institute of Technology.

Jackson M. L., Lim C. H., and Zelazny L. W. (1986) Oxides, hydroxides and aluminosilicates. In *Methods in Soil Analysis. Part 1-Physical and Mineralogical Methods* (ed. A. Klute), pp. 101–150. Amer. Soc. Agron. Inc.

Jefferson D. A., Tricker M. J., and Winterbottom A. P. (1975) Electron-microscopic and Mössbauer spectroscopic studies of iron-stained kaolinite minerals. *Clays Clay Min.* **23,** 355–360.

Jones R. C., Hudnall W. H., and Sakai W. S. (1982) Some highly weathered soils of Puerto Rico. 2. Mineralogy. *Geoderma* **27,** 75–137.

Kaplan D. I., Bertsch P. M., and Adriano D. C. (1995) Facilitated transport of contaminant metals through an acidified aquifer. *Groundwater* **33,** 708–717.

Kaplan D. I., Bertsch P. M., Adriano D. C., and Miller W. P. (1993) Soil-borne mobile colloids as influenced by water flow and organic carbon. *Environ. Sci. Tech.* **27,** 1193–1200.

Kodama H. and Ross G. J. (1991) Tiron dissolution method used to remove and characterize inorganic components in soils. *Soil Sci. Soc. Amer. J.* **55,** 1180–1187.

Lee S. Y., Hyder L. K., and Alley P. D. (1991) Microstructural and mineralogical characterization of selected shales in support of nuclear waste repository studies. In *Microstructure of Fine-grained Sediments* (ed. R. H. Bennett et al.), pp. 61–72. Springer-Verlag.

Leppard G. G. (1993) Evaluation of electron microscope techniques for the description of aquatic colloids. In *Environmental Particles* (ed. J. Buffle and H. P. vanLeeuwan), pp. 233–289. Intl. Union Pure Appl. Chem.

Liang L., McCarthy J. C., Jolley L. W., McNabb J. A., and Mehlhorn T. L. (1993) Iron dynamics: Transformation of Fe(II)/Fe(III) during injection of natural organic matter in a sandy aquifer. *Geochim. Cosmochim. Acta* **57,** 1987–1999.

Malengreau N., Muller J.-P., and Calas G. (1994) Fe-speciation in kaolins: A diffuse reflectance study. *Clays Clay Min.* **42,** 137–147.

McCarthy J. F., et al. (1993) Mobility of natural organic matter in a sandy aquifer. *Environ. Sci. Tech.* **27,** 667–676.

McCarthy J. F. and Zachara J. M. (1989) Subsurface transport of contaminants. *Environ. Sci. Tech.* **23,** 496–502.

McDowell-Boyer L. M. (1992) Chemical mobilization of micron sized particles in saturated porous media under steady flow conditions. *Environ. Sci. Tech.* **26,** 586–593.

Morel F. M. M. and Hering J. G. (1993) *Principles and Applications of Aquatic Chemistry.* Wiley.

Newman A. C. D. and Hayes M. H. B. (1990) Some properties of clays and of other soil colloids and their influence on soils. In *Soil Colloids and their Associations in Aggregates* (ed. M. F. DeBoodt), pp. 39–55. Springer Verlag.

Newman M. E., Elzerman A. W., and Looney B. B. (1993) Facilitated transport of selected metals in aquifer material packed columns. *J. Contam. Hydrol.* **14,** 233–246.

Oades J. M. (1984) Interactions of polycations of aluminum and iron with clays. *Clays Clay Min.* **32,** 49–57.

Penrose W. R., Polzer W. L., Essington E. H., Nelson D. M., and Orlandini K. A. (1990) Mobility of plutonium and americium through a shallow aquifer in a semiarid region. *Environ. Sci. Tech.* **24,** 228–234.

Perret D., Leppard G. G., Müller M., Belzile N., DeVitre R., and Buffle J. (1991) Electron microscopy of aquatic colloids: Nonperturbing preparation of specimens in the field. *Water Res.* **25,** 1333–1343.

Ronen D., Magaritz M., Weber U., and Amiel A. (1992) Characterization of suspended particles collected in groundwater under natural gradient flow conditions. *Water Resourc. Res.* **28,** 1279–1291.

Ryan J. N. and Gschwend P. M. (1990) Colloid mobilization in two Atlantic Coastal Plain aquifers, field studies. *Water Resourc. Res.* **26,** 307–322.

Ryan J. N. and Gschwend P. M. (1991) Extraction of iron oxides from sediments using reductive dissolution by titanium(III). *Clays Clay Min.* **39,** 509–518.

Ryan J. N. and Gschwend P. M. (1992) Effect of iron diagenesis on the transport of colloidal clay in an unconfined sand aquifer. *Geochim. Cosmochim. Acta* **56,** 1507–1521.

Ryan J. N. and Gschwend P. M. (1994) Effect of solution chemistry on clay colloid release from an iron oxide-coated aquifer sand. *Environ. Sci. Tech.* **28,** 1717–1726.

Santos M. C. D., Mermut A. R., and Ribeiro M. R. (1989) Submicroscopy of clay microaggregates in an oxisol from Pernambuco, Brazil. *Soil Sci. Soc. Amer. J.* **53,** 1895–1901.

Schahabi S. and Schwertmann U. (1970) Der Einflus von synthetischen Eisenoxiden auf die Aggregation zweier Losbodenhorizonte. *Z. Pflanzenernähr. Bodenkd.* **125,** 193–204.

Schindler P. W. and Stumm W. (1987) The surface chemistry of oxides, hydroxides, and oxide minerals. In *Aquatic Surface Chemistry* (ed. W. Stumm), pp. 83–110. Wiley.

Schwertmann U. (1964) Der Einflus von synthetischen Eisenoxiden des Bodens durch Extraktion mit Ammonium Oxalat-Lösung. *Z. Pflanzenernähr. Bodenkd.* **105,** 194–202.

Schwertmann U. and Kampf N. (1985) Properties of goethite and hematite in kaolinitic soils of southern and central Brazil. *Soil Sci.* **139,** 344–350.

Schwertmann U. and Taylor R. M. (1989) Iron oxides. In *Minerals in Soil Environments* (ed. J. B. Dixon and S. B. Weed), 2nd ed., pp. 379–427.

Seaman J. C., Bertsch P. M., and Miller W. P. (1995) Chemical controls on colloid generation and transport in a sandy aquifer. *Environ. Sci. Tech.* **29,** 1808–1815.

Short S. A., Lowson R. T., and Ellis J. (1988) $^{234}U/^{238}U$ and $^{230}Th/^{234}U$ activity ratios in the colloidal phases of aquifers in lateritic

weathered zones. *Geochim. Cosmochim. Acta* **52,** 2555–2563.
Smart P. and Tovey N. K. (1981) *Electron Microscopy of Soils and Sediments: Examples.* Clarendon Press.
Sposito G. (1984) *The Surface Chemistry of Soils.* Oxford Univ. Press.
Thompson M. and Walsh J. N. (1989) *Handbook of Inductively Coupled Plasma Spectrometry.* Chapman and Hall.
van Olphen H. (1977) *An Introduction to Clay Colloid Chemistry.* 2nd ed. Wiley.
Wada K. (1989) Allophane and Imogolite. In *Minerals in Soil Environments* (ed. J. B. Dixon and S. B. Weed), 2nd ed., pp. 1051–1088. Amer. Soil Sci. Soc.
Wang H. D., White G. N., Turner F. T., and Dixon J. B. (1993) Ferrihydrite, lepidocrocite, and goethite in coatings from east Texas vertic soils. *Soil Sci. Soc. Amer. J.* **57,** 1381–1386.
Wilding L. P. and Drees L. R. (1973) Scanning electron microscopy of opaque opaline forms isolated from forest soils in Ohio. *Soil Sci. Soc. Amer. J.* **37,** 647–650.
Wilding L. P., Hallmark C. T., and Smeck N. E. (1979) Dissolution and stability of biogenic opal. *Soil Sci. Soc. Amer. J.* **43,** 800–802.
Williams T. M. and McCarthy J. F. (1991) Field-scale tests of colloid:facilitated transport. Proc. Natl. Res. Devel. Conf. Contr. Hazard. Mater. 179–184.
Yariv S. and Cross H. (1979) *Geochemistry of Colloid Systems.* Springer-Verlag.